Design and experiment of a human-machine cooperative Chinese wolfberry harvester

Chenghao Pan[1,2], Yuxuan Cao[1], Zhicheng Tian[2], Jing He[2], Song Mei[1*], Zhiyu Song[3*]

(1. *Nanjing Institute of Agricultural Mechanization, Ministry of Agriculture and Rural Affairs, Nanjing 210014, China*;
2. *School of Mechanical Engineering, Nanjing University of Science and Technology, Nanjing 210094, China*;
3. *Key Laboratory of Modern Agricultural Equipment, Ministry of Agriculture and Rural Affairs, Nanjing 210014, China*)

Abstract: Against the background of large-scale and high-quality development of the Chinese wolfberry industry, vibration-based mechanized harvesting methods still face challenges in achieving both low-damage and precise harvesting of fresh wolfberries in the short term. Human-machine collaborative harvesting provides a feasible approach to improving the adaptability of mechanized fresh wolfberry harvesting under current conditions. To overcome the problems of inclined trunks, ground-hugging fruiting branches, and complex field environments in traditional wolfberry cultivation, a human-machine collaborative wolfberry harvester was developed to address the issues of insufficient field trafficability, low fruit-catching efficiency, and high fruit damage rate. The bilateral fruit-catching devices were designed with adjustable width and height to adapt to field conditions and improve inter-row operational performance. The adjustable width enabled the catching devices to close around the trunk center, thereby reducing fruit loss during catching. Collision kinematics analysis and simulation were conducted considering fruit falling height, catching plate inclination angle, and cushioning material selection. Under the constraint of non-destructive fruit catching, a flexible catching plate was designed to achieve low-damage fruit collection. Furthermore, the conveying and pneumatic separation mechanisms were optimized to establish an integrated “catching-conveying-separation” technology scheme for fruit collection and impurity removal. A portable vibration harvesting device was developed, and a spring-balanced auxiliary suspension structure was adopted to reduce operator holding load and improve human-machine collaborative operation comfort. Finite element analysis was performed to verify the strength and stiffness of the machine frame structure, and field performance tests were conducted to evaluate the travelling stability and harvesting performance of the prototype. The results showed that the prototype met the design requirements under sandy loam and soft-ground conditions, achieving stable travelling performance and completing operations such as in-situ turning. Under typical operating conditions, the fruit damage rate during harvesting was approximately 2.27%, and the actual damage rate after 24 h storage was 4.07%. The impurity removal rate of the pneumatic separation device reached 97.5%, with a fruit loss rate of 0.3% during separation. In conclusion, the developed human-machine collaborative wolfberry harvester can meet the harvesting requirements of fresh wolfberries and provide an effective solution for alleviating labor shortages.

Keywords: Chinese wolfberry, human-machine cooperative, tracked harvesting platform, fruit collection and pneumatic separation, fruit damage rate
DOI: 10.25165/j.ijabe.20261904.10678

Citation: Pan C H, Cao Y X, Tian Z C, He J, Mei S, Song Z Y. Design and experiment of a human-machine cooperative Chinese wolfberry harvester. Int J Agric & Biol Eng, 2026; 19(4): 79–87.

1 Introduction

Chinese wolfberry is an important medicinal and edible berry crop in China[1]. It is mainly cultivated in trellis or high-density planting systems with narrow row spacing and has multiple flowering and fruiting cycles in spring, summer, and autumn[2]. Its fruits are mechanically fragile[3], while harvesting remains highly dependent on manual labor and existing mechanized equipment has limited field adaptability[4]. Improving orchard-machine compatibility and achieving low-damage harvesting are therefore key requirements for mechanized Chinese wolfberry harvesting[5,6].

At present, Chinese wolfberry harvesting equipment is mainly classified into portable and self-propelled types. Harvesting methods include vibration, brushing, pneumatic suction, and cutting, among which vibration-based harvesting is the most widely used. Jiang et al.[7] developed a flexible comb-brush harvesting machine integrating fruit detachment, collection, and impurity separation functions, whereas Yu et al.[8] designed a comb-brush picker with flexible picking teeth and analyzed its fruit-tooth collision characteristics. Mei et al.[9] designed the 4GQF-2200 machine, which combines a tunnel-type profiling reciprocating vibration system with a flexible fruit-catching, anti-leakage, and collecting system. Zhao and Yan[10] proposed a vertically cutting self-propelled harvester that adopted a clamping-plate-cutter cooperative mechanism to reduce accidental injury to the basal part of the plants under branch-swaying conditions. In addition, Zhang et al.[11] optimized the operating parameters of a Chinese wolfberry pneumatic separation device to improve fruit-leaf separation performance.

Received date: 2026-06-04 **Accepted date:** 2026-07-27

Biographies: Chenghao Pan, MS candidate, research interest: mechanical design, Email: panchenghao@njust.edu.cn; **Yuxuan Cao**, MS candidate, research interest: agricultural equipment engineering, Email: 2225284705@qq.com; **Zhicheng Tian**, PhD candidate, research interest: agricultural equipment and robot, Email: tianzhicheng@njust.edu.cn; **Jing He**, MS candidate, research interest: mechanical engineering, Email: 2799398831@qq.com.

***Corresponding author: Song Mei**, Associate Professor, research interest: agricultural mechanization engineering for fruits. Nanjing Institute of Agricultural Mechanization, Ministry of Agriculture and Rural Affairs, Nanjing 210014, China. Tel: +86-15366092940, Email: meisong@caas.cn; **Zhiyu Song**, Professor, research interest: agricultural mechanization engineering. Key Laboratory of Modern Agricultural Equipment, Ministry of Agriculture and Rural Affairs, Nanjing 210014, China. Tel: +86-15366093037, Email: songzhiyu@caas.cn.

Therefore, a human-machine cooperative Chinese wolfberry harvester was developed for trellis-grown orchards. The crawler chassis, fruit-catching and conveying mechanisms, pneumatic separation device, and portable vibration harvesting unit were designed, and field tests were conducted to evaluate trafficability, fruit damage, and pneumatic separation performance.

2 Overall structure and working principle

Previous studies demonstrated the feasibility of integrating fruit detachment, catching, conveying, pneumatic separation, and collection on a field harvesting platform[12,13]. The technical parameters of the human-machine cooperative Chinese wolfberry harvester are listed in Table 1. The machine mainly consists of three parts: the frame, fruit-catching and collection platform, and control system, as shown in Figure 1. The fruit-catching and collection platform includes the upper and lower obstacle-avoidance mechanisms, left and right obstacle-avoidance mechanisms, conveying devices, mesh fruit-catching devices, flexible fruit-catching plates, flexible retractable fruit-retaining fabrics, pneumatic separation devices, and fruit-box frames. The control system mainly consists of a touchscreen and a joystick. The joystick is used to control the traveling and steering of the crawler platform, while the touchscreen is used to control the adjustment and coordinated operation of the fruit-catching and collection platform.

Table 1 Technical parameters of the human-machine cooperative Chinese wolfberry harvester

Item	Parameter
Overall dimensions (L×W×H)/mm	2350×2300×2150
Machine mass/kg	1400
Drive motor power/kW	2.4
Track width (single side)/mm	180
Ground contact pressure/MPa	0.0346
Ground contact length/mm	1100
Steering mode	Pivot steering
Travel range of upper/lower obstacle-avoidance mechanism (single side)/mm	0-200
Travel range of left/right obstacle-avoidance mechanism (single side)/mm	0-150
Maximum traveling speed of the machine/km·h^{-1}	1.125

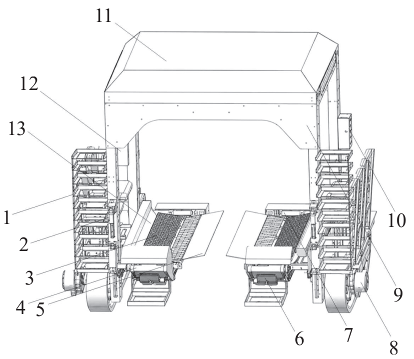

1. Fruit collection box frame 2. Upper and lower obstacle-avoidance mechanisms 3. Mesh fruit-catching device 4. Conveying device 5. Flexible fruit-catching plate 6. Blower 7. Left and right obstacle-avoidance mechanisms 8. Traveling mechanism 9. Gantry frame 10. Control box 11. Lithium battery pack and motor drivers 12. Touchscreen 13. Flexible retractable fruit-retaining cloth

Figure 1 Overall structure of the human-machine cooperative Chinese wolfberry harvester

The working principle is as follows. Before operation, the initial heights of the upper and lower obstacle-avoidance mechanisms and the spacing between the left and right obstacle-avoidance mechanisms are adjusted according to the plant morphology, branch distribution, and fruit distribution. One fruit-catching plate is then extended toward the trunk through the touchscreen. After the one-key closing function is activated, the fruit-catching plate on the opposite side automatically extends until the two plates meet near the trunk, forming a complete fruit-catching area.

During harvesting, operators on both sides of the machine selectively harvest mature Chinese wolfberry fruits using portable vibration harvesters. The detached fruits are received by the mesh fruit-catching devices, flexible fruit-catching plates, and flexible retractable fruit-retaining fabrics. The fruit-retaining fabrics extend synchronously with the fruit-catching plates to enlarge the catching area and intercept scattered fruits. After harvesting of the current plant is completed, the one-key collection function is activated through the touchscreen. The mesh fruit-catching devices on both sides rotate in opposite directions about their respective shafts, forming gaps between adjacent fruit-catching units. The fruits retained on the mesh screens then fall through the gaps onto the conveyor belts under gravity. Meanwhile, the conveyor belts and blowers are activated simultaneously to continuously transport the fruits and impurities such as leaves to the discharge end, where pneumatic separation is performed before the fruits enter the collection boxes.

After conveying, the one-key retraction function returns both fruit-catching plates to their initial positions and simultaneously stops the conveyor belts and blowers, completing one harvesting cycle.

3 Design of key components

3.1 Structural and parameter design of the crawler assembly

A conventional four-wheel-and-one-track crawler traveling system was adopted to improve terrain adaptability and field trafficability, as shown in Figure 2.

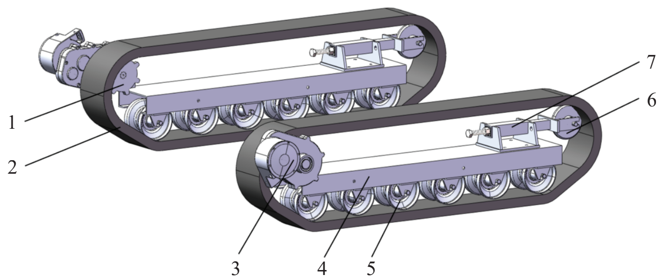

1. Drive sprocket 2. Track 3. Motor and reducer 4. Frame 5. Road wheel 6. Tension wheel 7. Tensioning device

Figure 2 Schematic diagram of the rubber trapezoidal crawler traveling device

3.1.1 Basic chassis parameter design

The rubber track width w, the ground pressure P of the entire machine, the track pitch t, and the total track length L can be calculated using the following equation:

$$\begin{cases} w=(0.9\sim 1.1)\times 209\times \sqrt[3]{F} \\ F=\dfrac{1}{2}M \\ P=\dfrac{M\times 10^3\times 9.8}{L_j\times 2w}=0.0346\ \mathrm{MPa} \\ t=(10\sim 23)\times \sqrt[4]{\dfrac{M\times 10^3}{2}}=51.4\sim 118.3\ \mathrm{mm} \\ L=2L_j+2zt+200=3408\ \mathrm{mm} \end{cases} \tag{1}$$

where, F is the load borne by a single track, t; M is the total machine mass, approximately 1.4 t; L_j is the track ground contact length, mm; z is the number of teeth on the drive sprocket, which was selected as 7.

A 180 mm-wide rubber track was selected for each side, and the ground contact length was 1100 mm. The track pitch was rounded to 72 mm. The front-end inclination angle of the inverted-trapezoidal track was designed as 30°, the length of each track was 3408 mm, and a wedge-pattern track with a tread height of 20 mm was selected.

3.1.2 Crawler system design

The pitch-circle diameter of the drive sprocket d_k, the addendum circle diameter d_a, and the diameter of the tension wheel d_z can be calculated by:

$$\begin{cases} d_k = \dfrac{t}{\sin\left(\dfrac{180}{z}\right)} \approx 166\ \text{mm} \\ d_a = d_k + 2T - 5 = 191\ \text{mm} \\ d_z = 0.9 d_a \approx 172\ \text{mm} \end{cases} \tag{2}$$

where, d_k is the pitch-circle diameter; d_a is the addendum circle diameter; T is the track thickness, 15 mm. The drive sprocket was made of 50 Mn, and the teeth were strengthened by medium-frequency quenching and low-temperature tempering. Six pairs of road wheels with a diameter of 160 mm were selected.

3.1.3 Calculation of crawler traction

The required traction of a single-side track was calculated for pivot steering on level ground and straight-line travel on the maximum design slope, and the larger value was adopted as the design traction force. The corresponding resistance components and required traction forces can be calculated as:

$$\begin{cases} F_1 = \mu_{\text{soil}} m_v g \\ F_1' = \mu_{\text{soil}} m_v g \cos\alpha \\ M_2 = \dfrac{\mu_{\text{turn}} m_v g L_j}{8} \\ F_2 = \dfrac{2\beta M_2}{B} \\ F_3 = m_v g \sin\alpha \\ F_4 = 0.06 m_v g \\ T_{\text{turn}} = \dfrac{F_1 + F_4}{2} + F_2 \\ T_{\text{slope}} = \dfrac{F_1' + F_3 + F_4}{2} \\ T = \max\left(T_{\text{turn}}, T_{\text{slope}}\right) \end{cases} \tag{3}$$

where, F_1 is the total soil deformation resistance of the machine on level ground, N; F_1' is the total soil deformation resistance on a slope, N; μ_{soil} is the soil resistance coefficient, taken as 0.15; m_v is the total mass of the machine, 1400 kg; g is the gravitational acceleration, 9.8 m/s^2; α is the maximum design climbing angle, 30°; M_2 is the turning resistance moment of a single track, N·m; μ_{turn} is the track turning resistance coefficient, taken as 1; L_j is the ground-contact length of a single track, 1.1 m; F_2 is the additional traction force required by a single track during pivot steering, N; B is the track gauge, 1.8 m; β is the additional resistance coefficient, taken as 1.12; F_3 is the grade resistance of the machine, N; and F_4 is the internal track resistance, N.

The calculated traction force required for pivot steering on level ground was 3788.2 N per track, whereas that required for straight-line travel on the maximum design slope was 4732.7 N per track. Therefore, the design traction force of a single-side track was taken as 4732.7 N.

3.1.4 Parameter calculation for the drive motor and reducer

The required output torque T_d, maximum rotational speed n, output power P, and reducer transmission ratio i of the single-side drive system can be expressed as:

$$\begin{cases} T_d = \dfrac{T R_k}{\eta_1} = 479\ \text{N}\cdot\text{m} \\ n = \dfrac{\omega}{2\pi} = 36.77\ \text{r/min} \\ P = \dfrac{T_d n}{9550\eta_2} = 1.98\ \text{kW} \\ i = \dfrac{2\pi R_k 3.6 \eta_d \eta_j n}{60 V_{\max}} = 50.6 \end{cases} \tag{4}$$

where, η_1 is the output efficiency of the drive sprocket, which was taken as $\eta_1 = 0.82$ under the limiting condition; considering a speed margin, the maximum vehicle speed $V_{\max}$ was calculated as 1.15 km/h. η_2 is the efficiency of the traveling transmission mechanism, taken as $\eta_2 = 0.93$. η_d is the drive efficiency of the motor, taken as $\eta_d = 0.98$; and η_j is the transmission efficiency of the reducer, taken as $\eta_j = 0.95$.

According to the calculation results, a 130WD-M07730-48V brushless DC motor was selected, with a working voltage of 48 V, rated power of 2.4 kW, rated torque of 7.7 N·m, and rated speed of 3000 r/min. An RV110-50 worm-gear reducer with a reduction ratio of i = 1:64 was selected. A dual-motor drive system was adopted[14], with a crawler track gauge of 1800 mm.

3.2 Design of the fruit-catching and conveying components

3.2.1 Kinematic analysis of fruit falling and collision

During Chinese wolfberry harvesting, the instantaneous fruit-detachment force F can be expressed based on the forces acting at the connection between the fruit and the pedicel as:

$$\begin{cases} F = F_{\text{cf}} + F_{\text{in}} + G\cos\theta_i \\ F_{\text{cf}} = m\omega^2 r_g \\ F_{\text{in}} = m a_g = m\dfrac{\Delta V}{\Delta t} \end{cases} \tag{5}$$

where, F_{cf} is the instantaneous centrifugal force acting on the Chinese wolfberry fruit, N; F_{in} is the instantaneous inertial force acting on the Chinese wolfberry fruit, N; θ_i is the angle between the gravity direction and the inertial force direction of the fruit, °; m is the fruit mass, kg; ω is the angular velocity of fruit rotation, rad/s; r_g is the distance between the fruit centroid and the branch, m; a_g is the instantaneous acceleration of the fruit, m/s^2; ΔV is the instantaneous velocity change of the fruit, m/s; and Δt is the time interval of the instantaneous velocity change, s.

Reciprocating-vibration studies have shown that Chinese wolfberry detachment is governed by the combined effects of branch vibration response, fruit inertial force, vibration frequency, and amplitude[15]. Based on the mechanical model established above and the adopted calculation parameters, the maximum fruit velocity at detachment was estimated to be approximately 2 m/s.

The motion state of Chinese wolfberry at the highest point can be expressed as:

$$\begin{cases} V_0 \sin\gamma - gt = 0 \\ H_1 = \dfrac{1}{2}gt^2 = \dfrac{V_0^2 \sin^2\gamma}{2g} \end{cases} \tag{6}$$

where, V_0 is the initial velocity at fruit detachment, $V_0 = \dfrac{2m}{s}$; γ is the angle between the initial velocity and the horizontal direction, (°); and H_1 is the upward displacement of the fruit, m.

The motion state of Chinese wolfberry at impact can be expressed as:

$$\begin{cases} H_1 + H_0 = \frac{1}{2}gt^2 \\ V_y = gt = \sqrt{2g(H_1+H_0)} = \sqrt{V_0^2\sin^2\gamma + 2gH_0} \\ V = \sqrt{V_x^2+V_y^2} = \sqrt{V_0^2\cos^2\gamma + V_0^2\sin^2\gamma + 2gH_0} = \sqrt{V_0^2 + 2gH_0} \\ \theta = \arctan\frac{V_y}{V_x} \end{cases} \tag{7}$$

where, V_y is the vertical velocity of the Chinese wolfberry fruit when it collides with the fruit-catching plate, m/s; H_0 is the distance between the fruit and the fruit-catching plate at detachment, m; V is the maximum velocity at impact, m/s; and θ is the collision angle, (°). A maximum fruit drop height of 1.3 m was selected. The maximum velocity of the Chinese wolfberry fruit when contacting the fruit-catching plate was calculated to be 5.4 m/s.

3.2.2 Selection and verification of flexible buffer materials

Leather was selected as the cushioning material and supported by steel wires with a length of 150 mm and a stacked thickness of 10 mm. Previous studies have investigated fruit impact bruising and cushioning during mechanical harvesting[16-18]. ANSYS was used to simulate the fruit-plate collision after fruit detachment, as shown in Figure 3. The simulated impact force increased overall with the collision angle, with a maximum value of 1.6 N, which was lower than the fruit damage threshold of 1.94 N.

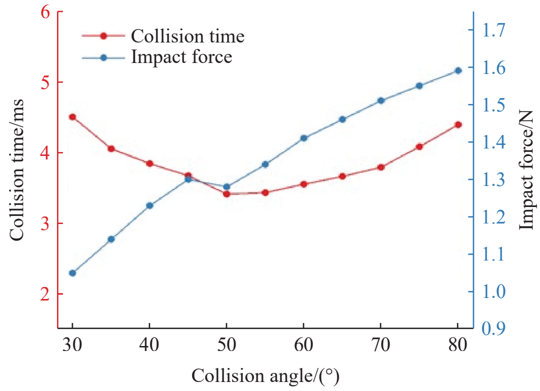

Figure 3 Simulation results of Chinese wolfberry collision motion after fruit detachment

Under the conditions of a fruit-catching plate inclination angle of 35°, leather cushioning material, and a fruit drop height of 1.3 m, the collision simulation results are shown in Figure 4. The maximum impact force between the Chinese wolfberry fruit and the fruit-catching plate was 1.14 N. Based on the simulation results, a lower collision angle could effectively reduce the impact force during fruit collision and decrease fruit damage. Therefore, considering fruit rolling requirements and installation space, the final inclination angle of the fruit-catching plate was set to 30°.

3.2.3 Selection of the power drive unit for the fruit-catching plate

A rotary drive motor was used to swing the fruit-catching plate. The calculation equation for the total motor torque T_j and input power P_j can be expressed as:

$$\begin{cases} T_j = (m_j + m_f)gr_z + (m_j+m_f)\alpha r_z^2 \\ P_j = \frac{T_j\omega_j}{\eta_m} \end{cases} \tag{8}$$

where, m_j is the mass of the fruit-catching plate, kg; m_f is the load mass on the fruit-catching plate, kg; r_z is the distance from the center of gravity to the rotation axis, m; α is the angular acceleration, rad/s²; ω_j is the maximum angular velocity, rad/s; and η_m is the motor efficiency, generally taken as 0.9.

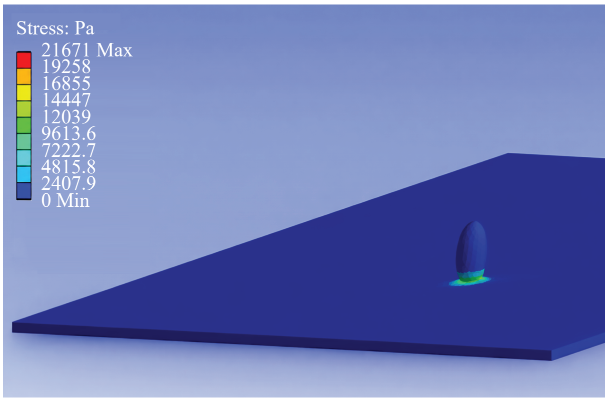

Figure 4 Equivalent stress contours from the simulation of Chinese wolfberry collision motion after fruit detachment

The fruit-catching plate has a length of 1460 mm and a width of 380 mm, yielding a mass of 2.56 kg. The load mass is 2 kg, the distance from the center of gravity to the rotation axis is 63 mm, the angular acceleration is π rad/s², and the maximum angular velocity is π rad/s. The required maximum torque is $T_{\max} = 2.88$ N·m and the power is 10.05 W. According to the calculation results, a Leadshine D57CM31 stepper motor was selected, with a torque of 3.1 N·m and a rated current of 5.6 A. An NMRV30 worm-gear reducer was selected with a reduction ratio of 10:1, and the reduced torque of the motor was 31 N·m.

3.2.4 Structural design of the conveyor belt

A PVC conveyor belt with a width of 260 mm and a thickness of 10 mm was adopted with an inclination angle of 30°. Transverse cleats with a spacing of 300 mm and a height of 20 mm were arranged to prevent fruit rollback. A retractable anti-drop device was installed to reduce fruit loss during transfer. The total traction force F_g, maximum torque $T_{\max}$, sprocket rotational speed ω_c, and output power P_d of the conveyor drive motor can be expressed as:

$$\begin{cases} F_g = (m_{tf}+m_{tw})g\sin\alpha + \mu_z\left[(m_{tf}+m_{tw})g\cos\alpha + (m_{sf}+m_{sw})g\right] \\ T_{\max} = kF_gR_l \\ \omega_c = \frac{V_c}{R_c} \\ P_d = \frac{T_{\max}\cdot\omega_c}{\eta_c} \end{cases} \tag{9}$$

where, m_{tf} and m_{tw} represent the load mass of the lifting section of the conveyor and the mass of the lifting section itself, respectively, kg; g is the gravitational acceleration; α is the angle between the lifting section and the horizontal section of the conveyor, $\alpha = 30°$; μ_z is the empirical friction coefficient of the conveyor, taken as $\mu_z = 0.05$; m_{sf} and m_{sw} represent the load mass of the horizontal section of the conveyor and the mass of the horizontal section itself, respectively, kg; k is the safety factor, taken as $k = 2$; R_l is the sprocket radius of the conveyor, m; V_c is the designed operating speed of the conveyor, m/s; R_c is the end radius of the conveyor, m; and η_c is the total efficiency of conveyor drive system, $\eta_c = 0.9$.

PVC conveyor belt density is 1.3 g/cm³, so the mass of the lifting section is 1.2 kg, and that of the horizontal section is 5.2 kg. Under normal harvesting speed, the load mass of the lifting section is 0.7 kg, and that of the horizontal section is 3 kg. The end radius of the conveyor was designed as 0.03 m, and the sprocket radius driving the conveyor was 0.06 m. The calculated maximum motor torque is $T_{\max}$ = 1.99 N·m, and the motor output power is P_d = 43 W. An 86HBP118AL4-TKC stepper motor was selected with a rated current of 5 A. The reducer selected was NMRV40-5 with a reduction ratio of 5:1.

3.2.5 Design of the fruit-catching and conveying mechanism

The fruit-catching and conveying unit was designed for vertical and lateral adjustment to avoid interference with Chinese wolfberry plants. SolidWorks calculations showed that the total mass of the single-side fruit-catching and conveying unit was 36 kg, and the maximum fruit load capacity was 2 kg.

The required thrust F_d, horizontal and vertical travel L_x, L_z can be calculated by the following equation:

$$\begin{cases} F_d = \dfrac{(m_{jg}+m_{fz})g}{\eta} = 428.56\text{ N} \\ L_x \geq \dfrac{W_f - 2\times(L_s + 2L_b/3)}{2} \\ L_z \geq L_0 - L_{\min} \end{cases} \tag{10}$$

where, m_{jg} is the mass of the fruit-catching and conveying mechanism, kg; m_{fz} is the maximum fruit load capacity, kg; η is the mechanism efficiency, taken as 0.85; W_f is the inner width of the frame, mm; L_s is the width of the single-side fruit-catching and conveying mechanism, mm; L_b is the width of the fruit-catching plate, mm; L_0 is installation height at bottom of fruit-catching and conveying mechanism, mm; and $L_{\min}$ is the minimum allowable height at bottom of fruit-catching and conveying mechanism, mm.

The frame width was 1410 mm, the width of the single-side fruit-catching and conveying mechanism was 320 mm, the fruit-catching plate width was 380 mm, the installation height of the fruit-catching and conveying mechanism was 420 mm, and the minimum allowable height at the bottom of the fruit-catching and conveying mechanism was 250 mm. The calculated horizontal travel was 87.78 mm and the vertical travel was 170 mm. For horizontal movement, an XC800-A-H electric actuator was selected, with a maximum thrust of 400 N, stroke of 150 mm, and speed of 65 mm/s. For vertical movement, an LSTN-A DC electric actuator was selected, with a maximum thrust of 2000 N, stroke of 200 mm, and speed of 5 mm/s.

3.3 Design of the pneumatic separation device

Differences in morphology and mass between Chinese wolfberry fruit and impurities such as leaves lead to different motion characteristics under airflow. The pneumatic separation device was installed at the discharge end of the inclined conveyor. Force and motion analyses of the fruits and impurities were conducted according to the airflow direction, as shown in Figure 5.

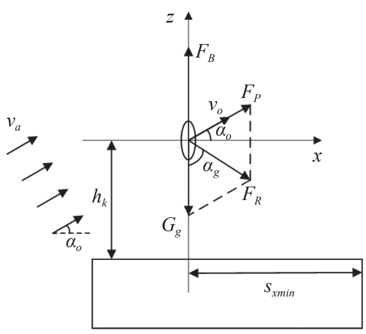

Figure 5 Mechanics analysis of the pneumatic separation

In the x-axis inclined airflow field, the motion of fresh Chinese wolfberry fruit is jointly governed by gravity G_g, oblique airflow action force F_p, and air buoyancy F_B, where F_B is much smaller than G_g and F_p and can therefore be neglected. The oblique airflow force F_p and the oblique airflow velocity $v(S)$ can be expressed as:

$$\begin{cases} F_p = C\rho' S_B v(S)^2 \\ v(S) = v_a - \mu_c S \end{cases} \tag{11}$$

where, C is the air drag coefficient; ρ' is the air density, kg/m³; S_B is the contact area between the airflow and the Chinese wolfberry fruit, m²; S is the displacement of the Chinese wolfberry fruit, m; v_a is the oblique airflow initial velocity, m/s; and μ_c is the airflow attenuation coefficient. Experiments showed that at a distance of 15 cm from the air outlet, the wind speed decreased by 5 m/s.

The trajectory of Chinese wolfberry fruit can be expressed as:

$$\begin{cases} h = \dfrac{G_g - F_p\sin\alpha_0}{2m}t^2 - v_0 t\sin\alpha_0 \\ s = \dfrac{F_p\sin\alpha_0}{2m}t^2 + v_0 t\cos\alpha_0 \\ S = \sqrt{h^2+s^2} \end{cases} \tag{12}$$

where, h is the downward displacement of the Chinese wolfberry fruit, m; G_g is the gravity of the Chinese wolfberry fruit, N; α_0 is the ejection angle of the lifting conveyor, (°); m is the mass of fresh Chinese wolfberry fruit, kg; t is the fruit ejection time, s; v_0 is the instantaneous ejection velocity of the fruit, m/s; and s is the forward displacement of the Chinese wolfberry fruit, m.

Under typical conditions, the air drag coefficient C was 0.6, the air density ρ was 1.225 kg/m³, the horizontal airflow contact area S_B was 1.96×10^{-5} m², the fresh Chinese wolfberry mass m was 0.0005 kg, the instantaneous ejection velocity v_0 was 0.6 m/s, and the ejection angle α_0 was 30°. The maximum allowable horizontal displacement between the conveyor end and the fruit collection box was $s_{x\max}$ =274 mm, and the vertical distance between the fruit ejection point and the upper edge of the fruit box frame was $h_{k\min}$ =184 mm. Under the constraints h>184 mm and s≤274 mm, the optimal initial oblique airflow velocity for pneumatic separation was calculated as v_a = 10.4 m/s.

A dual-blower configuration with a combined air duct was adopted. In ANSYS, the duct outlet pressure was set to 0 Pa, the wall was defined as a no-slip boundary, the air density was 1.225 kg/m³, the dynamic viscosity was 1.81×10^{-5} kg/(m·s), and the temperature was 20°C. The inlet velocity was iteratively adjusted until the outlet velocity reached 10.4 m/s, as shown in Figure 6.

The simulated outlet velocity was 10.4 m/s, corresponding to an inlet velocity of 4.69 m/s. Accordingly, a 36 W DC24 V blower providing an air velocity of 10.6 m/s was selected.

3.4 Design of the portable vibration harvesting unit

The portable vibration harvester mainly consists of a DC motor, coupling, crank-end bearing, slider, and vibrating fork, as shown in Figure 7a. The crank-slider mechanism converts motor rotation into high-speed reciprocating motion of the vibrating fork. Previous studies have shown that vibration parameters, moving-component mass, and structural configuration affect the detachment performance and energy consumption of Chinese wolfberry vibration harvesters[19-22].

To reduce the load associated with prolonged handheld operation, a spring-balancer-assisted suspension arrangement was adopted, as shown in Figure 7b. Mounted on the upper gantry frame, the spring balancer partially offsets the harvester weight, allowing the operator to mainly control its working position and vibration direction. The practical suspension and operation of the portable vibration harvester are shown in Figure 7c.

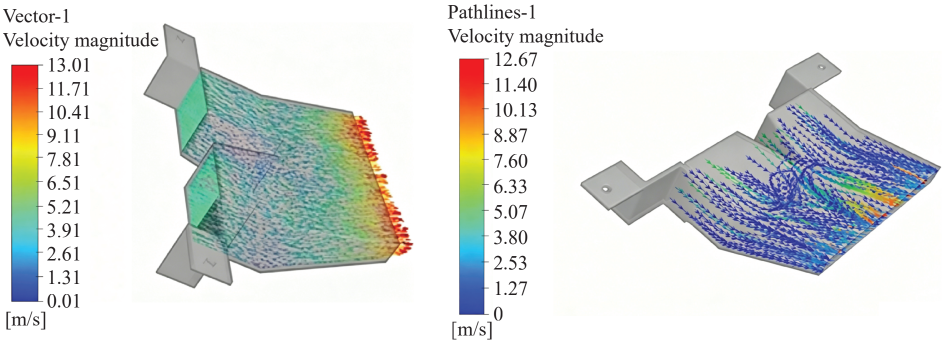

a. Air-velocity vector diagram of the duct b. Air-velocity streamline diagram of the duct

Figure 6 Simulation results of air velocity in the duct

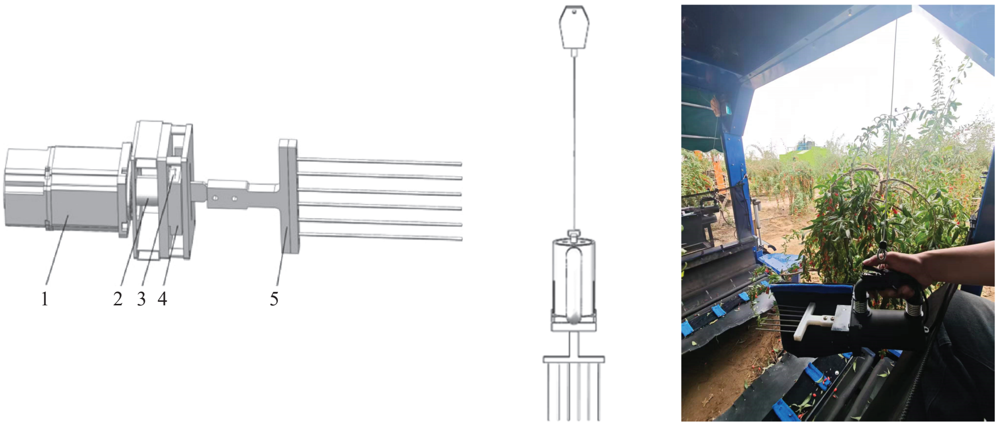

a. Structure of the portable vibration harvester b. Suspension arrangement with the spring balancer c. Practical operation of the portable vibration harvester

1. DC motor 2. Coupling 3. Crank-end bearing 4. Slider 5. Vibrating fork

Figure 7 Structure, suspension arrangement, and practical operation of the portable vibration harvester

From the perspective of force balance, the portable vibration harvester is mainly subjected to its own gravity, the upward balancing force provided by the spring balancer, and the guiding force applied by the operator. Assuming that the mass of the portable vibration harvester is m_h, its gravity can be expressed as $G_h = m_h g$. When the upward balancing force provided by the spring balancer is T_s, the effective handheld load borne by the operator can be expressed as:

$$F_h = G_h - T_s \tag{13}$$

where, F_h is the residual handheld load borne by the operator, G_h is the gravity of the portable vibration harvester, and T_s is the balancing force of the spring balancer. When T_s approaches G_h, most of the self-weight of the portable vibration harvester is balanced by the suspension device, and the operator only needs to provide a small guiding and positioning force.

3.5 Frame structural design and static analysis

As shown in Figure 8, the ANSYS simulation yielded a maximum equivalent stress of 74.749 MPa and a maximum deformation of 1.0455 mm under the prescribed static loads and torque. Both values were within the allowable limits, indicating that the frame satisfied the structural strength and stiffness requirements.

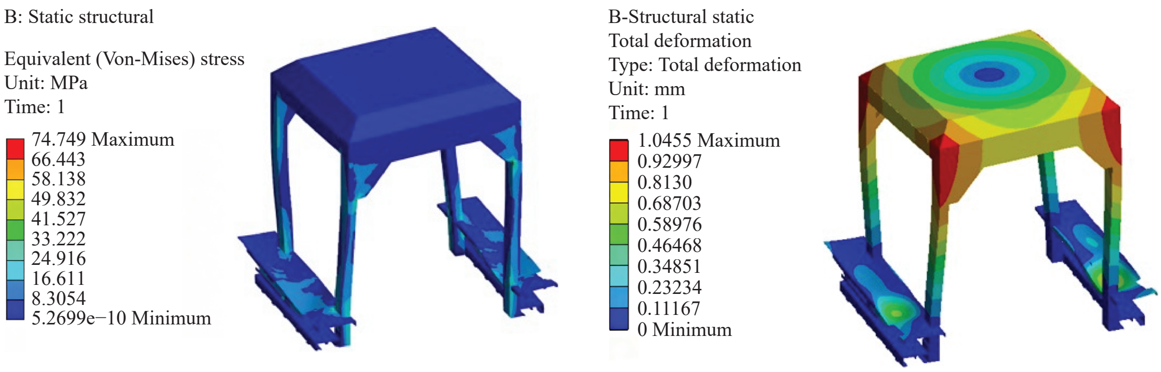

a. Stress distribution b. Total deformation distribution

Figure 8 Stress and total deformation distributions of the frame under load and torque

The gantry frame was fabricated from Q235 steel, and its static strength and stiffness were evaluated using finite element analysis[23]. A gravity load of 300 N was applied to the lithium battery pack and drivers on each side of the upper frame. The conveyor belt and fruit-catching mechanism on each side were subjected to a gravity load of 2000 N, while each operator seat and fruit collection box bore 1300 N and 400 N, respectively. These component loads were simplified as concentrated forces acting at their centers of mass.

3.6 Stability analysis of the machine

The rollover and sliding stability of the machine were analyzed based on its center-of-gravity position. SolidWorks calculations gave a center-of-gravity height of 0.895 m, with the center of gravity located at the midpoint of the track gauge and between the front and rear tracks, as shown in Figure 9.

The limiting lateral rollover angle α_{h_0} and the limiting lateral sliding angle β_0 can be calculated from force equilibrium as following equation:

$$\begin{cases} N_1 + N_2 = G_Z \cos\alpha_h \\ f_h = \mu(N_1 + N_2) = G_Z \sin\alpha_h \\ N_1 L_g = G_Z \cos\alpha_h \left[\dfrac{L_g}{2} - h\tan\alpha_h\right] \\ N_1 = \dfrac{G_Z\left(\dfrac{L_g}{2} - h\tan\alpha_h\right)\cos\alpha_h}{L_g} \\ \alpha_{h_0} = \arctan\dfrac{L_g}{2h} \\ \beta_0 = \arctan\mu \end{cases} \tag{14}$$

where, N_1 is the normal support force exerted by the slope on the right track during operation, N; N_2 is the normal support force exerted by the slope on the left track during operation, N; G_Z is the gravity acting on the machine, N; α_h is the limiting lateral rollover angle at which the machine does not overturn, (°); f_h is the lateral friction force acting on the machine, N; μ is the friction coefficient of the track on the slope; L_g is the track gauge, m; b is the track width, m; and h is the vertical distance between the center of gravity and the slope surface, m.

To ensure that the operating vehicle does not overturn laterally, it is necessary to satisfy $N_1 \geq 0$; when $N_1 = 0$, the limiting lateral rollover angle was calculated as 45.16°. Taking the track-slope friction coefficient μ =0.6, the limiting angle at which the machine does not laterally slide was calculated as 30.96°.

The limiting longitudinal rollover angle α_{z_0} can be calculated from force equilibrium as following equation:

$$\begin{cases} N = G_Z \cos\alpha_z \\ f_z = \mu N = G_Z \sin\alpha_z \\ N l_c = G_Z \cos\alpha_z \left(\dfrac{L_j}{2} - h\tan\alpha_z\right) \\ l_c = \dfrac{L_j}{2} - h\tan\alpha_z \\ \alpha_{z_0} = \arctan\dfrac{L_j}{2h} \end{cases} \tag{15}$$

where, N is the normal support force exerted by the slope on the track, N; α_z is the limiting longitudinal rollover angle at which the machine does not overturn, (°); f_z is the longitudinal friction force acting on the machine, N; l_c is the distance between the reaction force of the slope on the machine and point C, m; L_j is the track ground contact length, m.

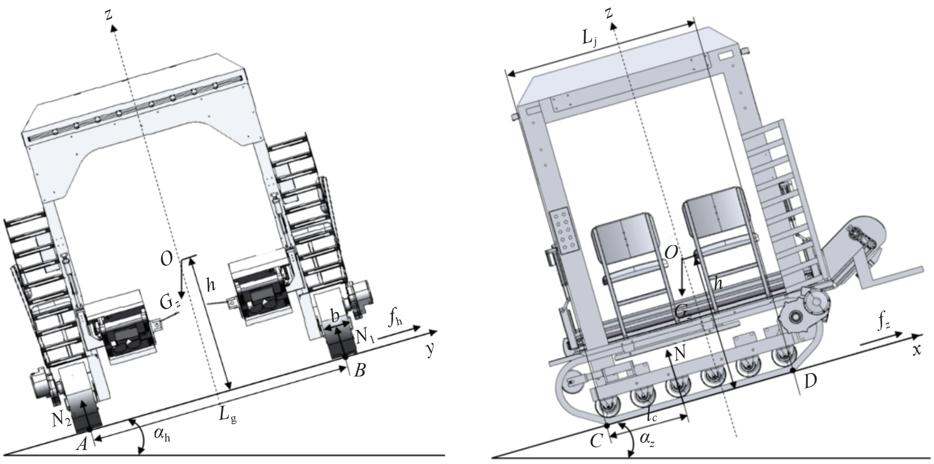

a. Lateral static force on the crawler on a slope b. Longitudinal static force on the crawler on a slope

Figure 9 Force diagram for stability analysis of the machine

To ensure that the operating vehicle does not overturn longitudinally, it is necessary to satisfy $l_c \geq 0$; when $l_c = 0$, the limiting longitudinal rollover angle was calculated as 31.57°. The longitudinal sliding condition is consistent with that in lateral travel, and the limiting angle at which the machine does not slide longitudinally was 30.96°.

4 Performance tests of the machine

4.1 Driving performance test of the machine

To evaluate the speed response of the prototype under remote control, traveling tests were conducted at low, medium, and high speed levels. The test course consisted of a 2 m acceleration section, a 10 m constant-speed test section, and a 2 m stopping buffer section. At each speed level, three groups of tests were conducted, with 10 repetitions per group. The mean travel time of each group was recorded, and the overall mean was used to calculate the traveling speed. The results are listed in Table 2.

Table 2 Field driving speed test results

Gear	No.	Time/s	Average time/s	Speed/ $m\cdot s^{-1}$	Theoretical velocity/$m\cdot s^{-1}$
	1	119			
Bottom speed gear	2	123	120	0.083	0.087
	3	118			
	1	51			
Medium speed gear	2	50	50.7	0.197	0.210
	3	51			
	1	34			
Top speed gear	2	33	35.3	0.283	0.313
	3	39			

The measured traveling speeds were lower than the theoretical values because of track slip and skidding.

In accordance with GB/T 3871.5—2022, the pivot-turning test was conducted on level hard pavement. The motors on both sides were controlled to rotate at equal speeds in opposite directions, enabling the prototype to complete a 360° pivot turn around its geometric center. The turning diameter was measured from the track marks on the ground, and the corresponding turning radius was calculated. Left- and right-turn tests were each conducted in three groups, with 10 repetitions per group. The group means are listed in Table 3.

Table 3 Minimum turning radius test

Turn toward	No.	Diameter/m	Average diameter/m	Turning radius/m
Left turn	1	2.21	2.20	1.10
	2	2.19		
	3	2.20		
Right turn	1	2.08	2.12	1.06
	2	2.10		
	3	2.18		

The mean turning radii for left and right turns were 1.10 and 1.06 m, respectively, and the overall mean turning radius was 1.08 m. This value was slightly larger than the theoretical value of 1.055 m because of track-ground friction and lateral slip. The overall mean turning radius was 1.08 m, slightly larger than the theoretical value of 1.055 m. This difference was mainly attributed to track-ground friction and lateral slip.

A field trafficability test was conducted in a Chinese wolfberry experimental orchard at the Wolfberry Science Research Institute, Ningxia Academy of Agriculture and Forestry Sciences. The orchard had a row spacing of approximately 3.1 m and a plant spacing of 0.9-1.1 m. The mature plants were approximately 1.4 m in height, with a transverse plant width of approximately 0.7 m. The ground consisted mainly of dry sandy soil interspersed with gravel, weeds, and local unevenness. The trafficability tests included uphill travel, cross-slope travel, ditch crossing, and step crossing. The uphill and cross-slope angles were set to 10°, 20°, and 30°; the ditch widths were 0.3, 0.4, and 0.5 m; and the rigid step heights were 7, 9, and 11 cm. The prototype entered each test section in a straight line at a constant low speed. Each test level was conducted in three groups, with 10 repetitions per group. A test was considered successful when the prototype completed the prescribed maneuver without continuous track slip, motor stalling, chassis grounding, structural interference, or loss of stability. Representative test scenes are shown in Figure 10, and the results are listed in Table 4.

a. Whole-machine field driving test

b. Hill-climbing and obstacle-crossing test

Figure 10 Field driving and trafficability tests of the machine

4.2 Harvesting performance test of the machine

4.2.1 Harvesting damage test and evaluation method

Damage tests were conducted on the third summer fruiting batch of seven-year-old Ningqi No. 1 Chinese wolfberry plants. The fruits were at normal harvest maturity and showed no visible damage before harvesting. The vibration amplitude and frequency of the portable vibration harvester were fixed at 15 mm and 20 Hz, respectively. Three repeated tests were conducted. In each repetition, 500 fruits were randomly sampled from the collection box for damage evaluation and then stored for 24 h under the same room-temperature and lighting conditions for re-evaluation. Fruit damage was classified into four grades: grade 0, no damage; grade 1, slight abrasion or bruising of less than 10 mm^2 without juice leakage; grade 2, bruising of no less than 10 mm^2 or skin breakage without obvious juice leakage; and grade 3, fruit cracking or obvious juice leakage[24]. The results are listed in Table 5.

Table 4 Results of the slope-travel and obstacle-crossing tests

Project	Data	Traffic situation
Climbing gradient/°	10	Passed
	20	Passed
	30	Passed
Lateral driving gradient/°	10	Passed
	20	Passed
	30	Passed
Crossing trench width/m	0.3	Passed
	0.4	Passed
	0.5	Passed
Crossing step height/cm	7	Passed
	9	Passed
	11	Passed

Table 5 Damage assessment results for harvested Chinese wolfberry fruits

	Damage grade immediately after harvesting /%				Damage grade at 24 h /%			
	0	1	2	3	0	1	2	3
Damage grade	98.0	1.2	0.6	0.2	96.0	2.8	1.0	0.2
	97.8	1.6	0.6	0	96.2	3.0	0.8	0
	97.4	1.4	0.8	0.4	95.6	2.6	1.2	0.6

The immediate total damage rate was 2.27%, increasing to 4.07% after 24 h. The increase occurred mainly in grade-1 damage, whereas grade-2 and grade-3 damage changed only slightly. This indicates that the increase mainly originated from the manifestation of latent damage during postharvest physiological and physical processes rather than from newly generated damage during the harvesting process.

4.2.2 Pneumatic separation performance test

An anemometer was used to measure the air velocity at the blower outlet, which was approximately 11.27 m/s. Preliminary tests indicated that effective leaf separation could be achieved at air velocities ≥8 m/s, while fruit blow-off remained limited below 16 m/s. For performance evaluation, a windproof tarpaulin was placed along the air-outlet side, and the materials collected in the fruit box and on the tarpaulin after pneumatic separation were weighed separately. At an air velocity of 11.27 m/s, the impurity removal rate was 97.5% and the fruit blow-off loss rate was 0.3%.

5 Conclusions

A human-machine cooperative Chinese wolfberry harvester was developed and evaluated through theoretical analysis, numerical simulation, and prototype tests. The main conclusions are as follows:

(1) The fruit-catching and conveying mechanisms were designed with vertical and lateral adjustability. At a fruit-catching

plate inclination angle of 35°, a fruit drop height of 1.3 m, and with leather as the cushioning material, the simulated maximum fruit impact force was 1.14 N, lower than the damage threshold of 1.94 N. Considering fruit rolling performance and installation constraints, the final inclination angle of the fruit-catching plate was set to 30°. Under the prescribed design loads, the maximum equivalent stress and deformation of the frame were 74.749 MPa and 1.0455 mm, respectively.

(2) The measured traveling speeds at the low, medium, and high speed levels were 0.083, 0.197, and 0.283 m/s, respectively. The mean pivot-turning radii for left and right turns were 1.10 and 1.06 m, respectively, with an overall mean of 1.08 m. The prototype successfully completed uphill and cross-slope tests at 30°, crossed a 0.5 m-wide ditch, and negotiated an 11 cm-high step.

(3) At a vibration amplitude of 15 mm and a vibration frequency of 20 Hz, the immediate total fruit damage rate was 2.27% immediately after harvesting and 4.07% after 24 h. At an airflow velocity of approximately 11.27 m/s, the pneumatic separation device achieved an impurity removal rate of 97.5% and a fruit blow-off loss rate of 0.3%.

Acknowledgements

This work was supported by the Innovation Team of Fruit, Vegetable and Tea Harvesting Technology and Equipment, Agricultural Science and Technology Innovation Program, Chinese Academy of Agricultural Sciences (CAAS-ASTIP-FVTH). The authors would like to thank the editor and reviewers for their valuable comments, time, and suggestions to improve the quality of the manuscript.

[References]

[1] Ma R H, Zhang X X, Ni Z J, Thakur K, Wang W, Yan Y M, et al. *Lycium barbarum* (Goji) as functional food: A review of its nutrition, phytochemical structure, biological features, and food industry prospects. Critical Reviews in Food Science and Nutrition, 2023; 63(30): 10621–10635.

[2] Li Y J, Hu Z Q, Zhang Y P, Wang J, Xu J H. Research progress of technology and equipment for mechanized harvest of wolfberry. Journal of Chinese Agricultural Mechanization, 2024; 45(5): 16–21,35. (in Chinese)

[3] Liu Y C, Liu J H, Zhao J, Wang F Y, Zhang H Y, Su X K, et al. Effects of different excitation parameters on mechanized harvesting performance and postharvest quality of first-crop organic goji berries in saline-alkali land. Agriculture, 2025; 15(13): 1377.

[4] Pan L W, Zhao D, Zhao J, Liu J H, Liu Y C, Feng Y K, et al. Analysis of fatigue characteristics in goji berry harvesting postures based on human factors and ergonomics. Forest Machinery & Woodworking Equipment, 2024; 52(7): 64–70,74. (in Chinese) doi: 10.13279/j.cnki.fmwe.2024.0075.

[5] Mei S, He J, Lyu X L, Song Z Y, Cao G Q, Shen C. Current status of orchard mechanization technologies and key development priorities in the 15th Five-Year Plan period. Int J Agric & Biol Eng, 2025; 18(6): 12–23.

[6] Pu Y J, Wang S M, Yang F Z, Ehsani R, Zhao L J, Li C S, et al. Recent progress and future prospects for mechanized harvesting of fruit crops with shaking systems. Int J Agric & Biol Eng, 2023; 16(1): 1–13.

[7] Jiang Y W, Han C J, Guo J X, Ma J G. Structural design and simulation modeling analysis of flexible comb-brush Chinese wolfberry harvester. Journal of Anhui Agricultural Sciences, 2024; 52(12): 192–196,221. (in Chinese)

[8] Yu Z H, Jiang F, Yang J H, Yan L, Wu J. Design and theoretical analysis of comb-type *Lycium barbarum* picking machine. Forest Machinery & Woodworking Equipment, 2024; 52(2): 30–36. (in Chinese)

[9] Mei S, Xiao H R, Shi Z G, Jiang Q H, Zhao Y, Ding W Q. Design and test of low-loss *Lycium barbarum* harvesting technology and equipment based on reciprocating vibration method. Journal of Chinese Agricultural Mechanization, 2019; 40(11): 100–105,208. (in Chinese)

[10] Zhao J, Yan S. A vertically cutting wolfberry picking machine: China Patent, CN116114466B. 2024-07-09. (in Chinese)

[11] Zhang H R, Kang F, Wang Y X, Tong S Y, Chen C C. Analysis and experiment of optimal operating parameters for goji berry wind separation. China Southern Agricultural Machinery, 2024; 55(17): 13–19. (in Chinese).

[12] Wang Y T, Yang C, Gao Y Y, Lei Y Q, Ma L F, Qu A L. Design and testing of an integrated *Lycium barbarum* L. Harvester. Agriculture, 2024; 14(8): 1370.

[13] Mei S, Tang D B, Shi Z G, Song Z Y, Tian Z C, Zhou R. Design and test of a Chinese wolfberry harvester using arrayed vibration units. Transactions of the CSAE, 2024; 40(23): 115–125. (in Chinese)

[14] Zhai L, Zhang X Y, Wang Z D, Mok Y M, Hou R F, Hou Y H. Steering stability control for four-motor distributed drive high-speed tracked vehicles. IEEE Access, 2020; 8: 94968–94983.

[15] Mei S, Wang J P, Song Z Y, Tang D B, Shen C. Mechanism and experimental study on the fruit detachment of Chinese wolfberry through reciprocating vibration. Int J Agric & Biol Eng, 2024; 17(2): 47–58.

[16] Jiang Y W, Chen Q Y, Wei N S. Determining the impact bruising of goji berry using a pendulum method. Horticulturae, 2025; 11(1): 14.

[17] Zhang Z, Igathinathane C, Li J B, Cen H Y, Lu Y Z, Flores P. Technology progress in mechanical harvest of fresh market apples. Computers and Electronics in Agriculture, 2020; 175: 105606.

[18] Sargent S A, Takeda F, Williamson J G, Berry A D. Harvest of southern highbush blueberry with a modified, over-the-row mechanical harvester: Use of soft-catch surfaces to minimize impact bruising. Agronomy, 2021; 11(7): 1412.

[19] Chen Y, Zhao J, Hu G R, Chen J. Design and testing of a pneumatic oscillating Chinese wolfberry harvester. Horticulturae, 2021; 7(8): 214.

[20] Mei S, Tang D B, Shi Z G, Song Z Y, Shen C. Energy consumption mechanism simulation and experimental study of reciprocating vibration for Chinese wolfberry picking. Int J Agric & Biol Eng, 2024; 17(4): 147–155.

[21] Tian Z C, Mei S, Song Z Y, Shen C, Pan C H, Tong Y F. Optimization design and test of vibration components in a Chinese wolfberry harvester. Int J Agric & Biol Eng, 2025; 18(6): 94–103.

[22] Chen Q Y, Zhang S X, Wei N S, Li P H, Hu G R, Chen J, et al. Design and optimization of torsion harvester of *Lycium barbarum* L. Int J Agric & Biol Eng, 2024; 17(4): 109–115.

[23] Chan T C, Ullah A, Roy B, Chang S L. Finite element analysis and structure optimization of a gantry-type high-precision machine tool. Scientific Reports, 2023; 13: 13006.

[24] Luo K N. Research on the dynamics of vibration harvesting and falling bruise of fruit for *Lycium barbarum*. MS thesis. Yinchuan: Ningxia University, 2023. (in Chinese) doi: 10.27257/d.cnki.gnxhc.2023.000634.